On the prediction of creep behaviour of alloy 617 using Kachanov-Rabotnov model coupled with multi-objective genetic algorithm optimisation

J. Choi [a,b], L. Bortolan Neto [a,b], R.N. Wright [c], J.J. Kruzic [b], O. Muránsky [a,b,*]

[a] *Australian Nuclear Science and Technology Organisation (ANSTO), Lucas Heights, NSW, Australia*
[b] *School of Mechanical and Manufacturing Engineering, University of New South Wales (UNSW Sydney), Sydney, NSW, 2052, Australia*
[c] *Idaho National Laboratory, Idaho Falls, ID, 83415, USA*

ARTICLE INFO

ABSTRACT

The accurate prediction of elevated-temperature creep behaviour of alloys is important for preventing catastrophic failure of systems operating under prolonged elevated temperature-stress conditions. Here, we couple the Kachanov-Rabotnov (K-R) creep model with a multi-objective genetic algorithm (MOGA) to predict the creep behaviour of Alloy 617 at $800°C$, $900°C$, and $1000°C$, under various stress conditions. It is shown that the MOGA-optimised K-R creep model can capture the overall elevated-temperature behaviour of the alloy at $800°C$ under a wide range of stress conditions. However, at $900°C$ and $1000°C$, oxidation leads to the atypical accumulation of creep plasticity, which the K-R model cannot account for. Nevertheless, it is shown that the proposed methodology of optimising the K-R model with a MOGA can consistently provide accurate results within the limits of the K-R model.

1. Introduction

Alloy 617 is a nickel-based superalloy with a wide range of applications in elevated-temperature systems across several industries, such as with intermediate heat exchanges in nuclear reactors [1]. Since these systems are required to operate at elevated temperatures and pressures, individual components are expected to undergo significant creep damage during their lifetime. For instance, intermediate heat exchangers in the next generation of nuclear reactors (Generation IV) are expected to operate at temperatures of up to 950°C and at pressures up to $7MPa$ [2–4]. These operating conditions lead to the accumulation of creep damage, which if left unmanaged can lead to the unexpected failure of a component or an assembly. Furthermore, excessive creep damage can significantly shorten the life of the system and compromise its overall economic viability. As such, the ability to predict the creep behaviour and accumulation of creep damage in various components of the system is of technological importance for engineers wishing to design and maintain an elevated temperature system.

Over the years, a number of empirical models have been developed to predict creep damage behaviour of different alloys in operational in-service conditions. The most widely used creep constitutive models are based on Norton's law [5], the Larson-Miller parameter [6], or the Manson-Haferd [7] methodology. These models require a large number of experimental creep data (i.e., time-to-failure, strain-to-failure, and minimum creep rate) to derive a master curve, which is then used to interpolate and/or extrapolate the creep life of an alloy under given temperature-stress conditions. We refer to these models as single-point models because they can only predict distinct points on the creep life/damage curve. Typically, the time-to-failure is predicted to indicate the remaining life and help perform fitness-for-service analysis. Multi-point models capable of capturing the full creep life/damage curve were developed to improve the accuracy of creep predictions and remove unnecessary conservatism of single-point models. Examples of the well-established multi-point creep models include the Ductility Exhaustion (DE) [8], Stress-Modified Ductility Exhaustion (SMDE) [9], and Strain-Energy Density (SED) [10] creep-damage models. While these models focus on the prediction of secondary creep behaviour, they can be coupled with other parametric models to account indirectly for the tertiary creep behaviour of alloys, as shown by Kan et al. in Ref. [11]. In contrast, the Kachanov-Rabotnov (K-R) creep model [12,13] was designed to inherently account for the multi-regime nature of creep in alloys and thus improve the overall predictions of creep behaviour. The K-R model accounts for the secondary and tertiary creep regimes, which

---

* Corresponding author. Australian Nuclear Science and Technology Organisation (ANSTO), Lucas Heights, NSW, Australia.
E-mail address: ondrej.muransky@ansto.gov.au (O. Muránsky).

Nomenclature

Creep-Related Parameters

t	Time
t_0	Initial time
T	Temperature
t_f	Time-to-failure
t_p	Time when primary creep regime begins
ε	Creep strain
ε_f	Strain-to-failure
$\dot{\varepsilon}_m$	Minimum creep rate
ε_p	Primary creep strain
ε_0	Initial creep strain
σ	Uniaxial stress
ω	Creep damage

Material Parameters

A	Norton law parameter

M	Tertiary creep damage material parameter
n	Norton law parameter
Φ	Tertiary creep damage material parameter
X	Tertiary creep damage material parameter

Optimisation Parameters

E_{t_f}	Objective function for time-to-failure means square error
E_ε	Objective function for creep strain means square error
E_{ε_f}	Objective function for strain-to-failure means square error
$E_{\dot{\varepsilon}_m}$	Objective function for minimum creep rate means square error
w_ε	Weight for creep strain objective function
w_{t_f}	Weight for time-to-failure objective function
w_{ε_f}	Weight for strain-to-failure objective function
$w_{\dot{\varepsilon}_m}$	Weight for minimum creep rate objective function

is considered acceptable for Alloy 617 as it only exhibits a limited primary creep regime [11,14,15]. However, the main challenge when using any multi-point constitutive model is finding the material parameters, which describe the observed creep behaviour of a given material. The strain and damage analytical method proposed by Stewart and Gordon [16] to obtain the K-R parameters is a step forward in avoiding a trial-and-error approach. However, it is somewhat intricate to employ as their method requires several intermediate regression analyses and subjective values, which makes it difficult to obtain generic parameters independent of applied stresses. In this paper, we present a methodology to find stress-independent K-R parameters which can be useful in describing long-term creep behaviour based on fittings to short-term creep tests.

Various numerical methodologies such as linear regression [11,15], simulated annealing [17], and artificial neural networks [18,19] have been employed to determine unknown material parameters in constitutive creep models with mixed results. Linear regression is the most widely used, due to its simplicity and effectiveness. However, its heavy reliance on the initial (starting) parameter values makes it inadequate for use in complex optimisation problems that involve finding multiple interdependent material parameters describing creep behaviour of a given alloy. Global optimisers like simulated annealing perform better, but their performances can be inconsistent, computationally intensive, and time-consuming [17]. In recent years, artificial neural networks in the form of multi-layer perceptrons, have shown significant promise as they have higher fault tolerance and better optimising capabilities [18, 19]. However, the training of neural networks requires a large amount of data, and their implementation can be complicated and require significant computational resources. Furthermore, the overfitting of training data can also result in unlikely predictions when extrapolating outside of the training range [20].

Population-based, stochastic, direct search algorithms, such as Evolutionary algorithms, are often employed in multi-objective optimisation problems and can potentially overcome the limitations of trial-and-error and Stewart and Gordon [16] approaches as these algorithms can optimise many parameters simultaneously across different datasets. Evolutionary algorithms are metaheuristic optimisation algorithms that were inspired by the mechanism of biological evolution and natural selection [21,22]. A large number of such algorithms have been developed, as highlighted in recent reviews [22–24]. Examples include the genetic algorithm, differential evolution, and particle swarm optimisation. Genetic algorithms, in particular, have been used to find multiple material parameters in various crystal plasticity constitutive laws [25]; however, to the authors' knowledge the extension of genetic algorithms

to creep model development has not yet been attempted.

In the present work, we employ a multi-objective genetic algorithm (MOGA) to determine stress-independent material parameters in the K-R creep model. This algorithm was selected due to its robustness and previous successful applications across multiple problems [21]. We calibrate the K-R model for Alloy 617 at 800°C, 900°C, and 1000°C, using experimental creep data generated at the Idaho National Laboratory (INL) [26]. We first employ the MOGA to find stress-independent K-R model's material parameters (A, n, M, φ, and χ) using both short- and long-term creep data. We then find the material parameters using only the short-term creep data and demonstrate the utility of the calibrated K-R model to predict the longer-term creep behaviour of the studied alloy extrapolating well beyond the training data. A non-exhaustive comparison between the MOGA and other optimisation techniques is out of scope of this paper as we are interested in quantitively evaluate the accuracy and repeatability of our methodology by direct comparison of the K-R model predictions with the experimental observations. We also conduct a parametric analysis of the MOGA optimisation settings and provide practical advice to achieve accurate and consistent optimisation results.

2. Methodology

Idaho National Laboratory (INL) undertook a decade long research program focused on the certification of Alloy 617 for elevated temperature nuclear pressure vessel applications operating at temperatures up to 950°C. To understand and ultimately predict the elevated-temperature behaviour of Alloy 617 at various in-service conditions, INL has performed creep tests at different temperature-stress conditions [26–29]. The current work builds upon this experimental work by exploring the capability of the K-R creep model in predicting the creep behaviour of Alloy 617. We first use the INL's experimental creep data to find the material parameters defining the K-R creep model (section 3) using MOGA optimisation (section 4), and then we test the accuracy of the K-R model predictions by direct comparison with the experimental measurements (section 5).

The INL-provided creep experimental data includes uniaxial creep curves of Alloy 617 conducted at constant temperature-stress conditions. These experiments were conducted to failure at 800°C (60MPa, 65MPa, 70MPa, 80MPa), 900°C (26MPa, 28MPa, 31MPa, 36MPa), and 1000°C (11MPa, 12MPa, 13MPa, 16MPa). The creep curves used in this study and all of the corresponding test conditions are summarised in Fig. 1. Note that the creep tests were conducted in air, which caused surface oxidation [30–32].
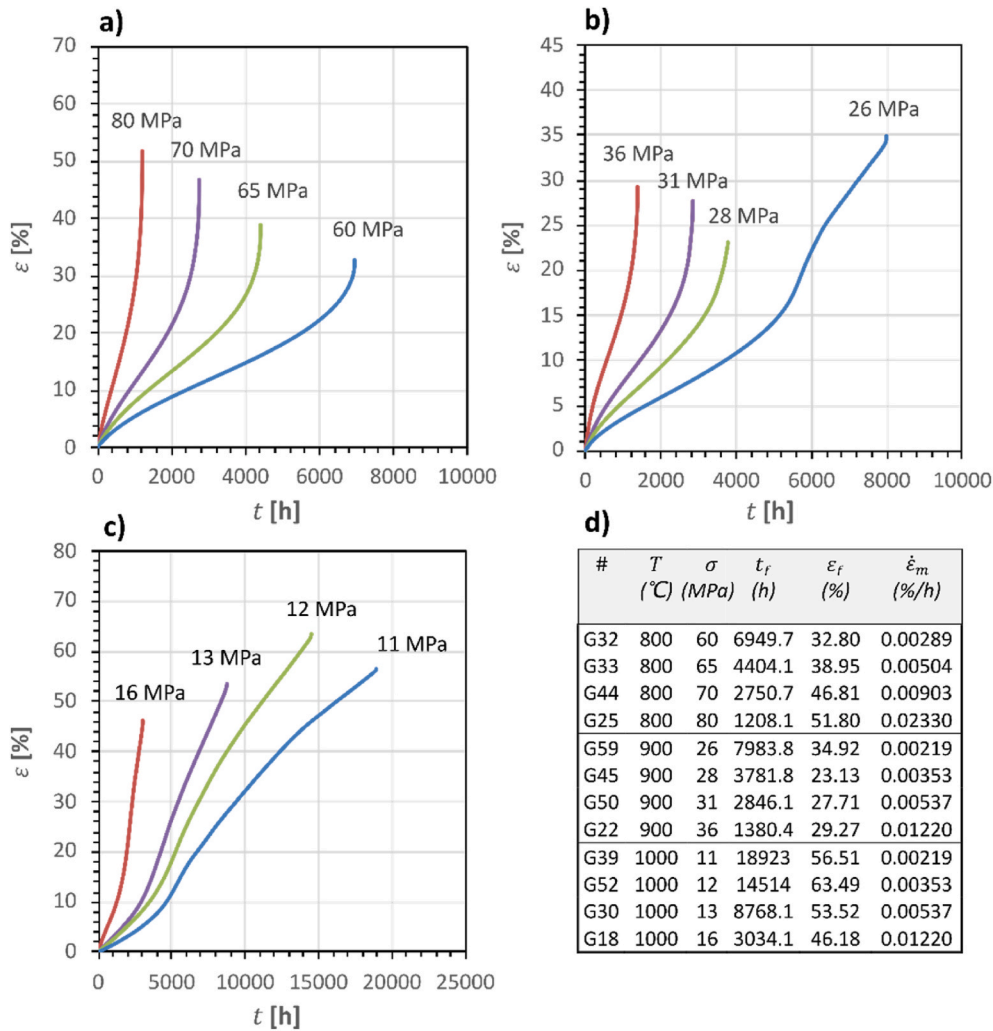
Fig. 1. Plots of observed, raw creep strain data for Alloy 617 from INL, for creep tests (a) at 800 °C, (b) at 900° C, and (c) at 1000°C, and (d) information about those creep tests.

As seen in Fig. 1b and c, the experimental creep curves at temperatures above 800°C and lower stresses exhibit atypical creep behaviour in their tertiary regimes. At those conditions, the creep curves have longer exposure times, whereby the kinetics of the alloy are more affected by the oxidation [31,33]. The creep curves shown in Fig. 1 also confirm that the creep life of Alloy 617 is spent predominantly in the secondary and tertiary creep regimes with a limited amount of the primary creep regime. This justifies using the K-R creep model, which omits the primary creep regime for the prediction of the creep behaviour. Because of this limitation, the experimental datapoints within the primary creep regime were disregarded in the calculation of the K-R parameters. To improve accuracy, we accounted for the primary creep region by implementing a strain offset, $\widehat{\varepsilon}_0$, for the predicted creep curves. For each experimental creep curve, we computed the tangent from the point in which minimum creep rate occurs. The value of $\widehat{\varepsilon}_0$ thus corresponds to the intercept between the tangent and the vertical axis, as shown in the schematic in Fig. 2.

After removing the primary creep region from the experimental data, we processed the experimental creep data to remove noise and create data input that was better suited for the MOGA. This involved fitting each creep curve to a 15-degree[1] polynomial and extracting 50 equally

spaced data points from the polynomials to use in the study. This was done because each INL dataset contains thousands of data points (approximately 9000), which can be accurately represented by 50 data points extracted from each polynomial. This technique reduces the number of calculations required, expediting the optimisation process without compromising the MOGA's performance. Finally, the INL datasets contain an uneven number of data points, in which the MOGA results would be biased by denser datasets. Representing each dataset with an equal number of data points removes this bias.

3. Kachanov-Rabotnov (K-R) creep model

The derivation of the K-R model used in this study follows Stewart et al. [16] – this involves the incorporation of Norton's power law [5] into the temperature-dependent K-R constitutive equations. Norton's power law is considered a single-point model used to estimate the minimum creep rate, $\dot{\varepsilon}_m$, of a material at given temperature and certain stress:

$$\dot{\varepsilon}_m = A\sigma^n \tag{1}$$

where σ is the uniaxial stress, and A and n are temperature dependent material parameters describing the secondary creep regime of the alloy. Hence, Norton's power law captures only the secondary creep behaviour – this is not suitable for Alloy 617, which can exhibit a long tertiary creep regime (Fig. 1), especially for the relatively higher-temperature,

---

[1] The fitting polynomial has to be of a high and odd degree ($2k + 1$, $k = 5,6,7$ …) to best conform to the shape of the typical Alloy 617 creep curve.
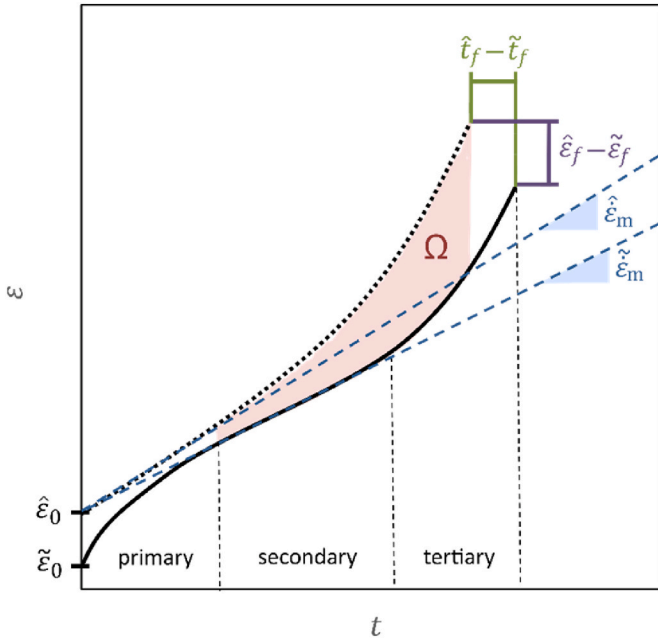
Fig. 2. Schematic of an observed creep curve (solid line) with the predicted creep curve (dotted line), annotated with the creep regimes, the initial creep strain ($\tilde{\varepsilon}_0$), the predicted creep strain offset ($\hat{\varepsilon}_0$), and relevant parameters tackled by the objective functions. The MOGA goal is to minimise the shaded area Ω along with the predicted and observed differences of time-to-failure and of strain-to-failure – i.e., $\hat{t}_f - \tilde{t}_f$ and $\hat{\varepsilon}_f - \tilde{\varepsilon}_f$. It is also aimed at aligning the predicted creep curve with the observed one, which is achieved by minimising the difference between the observed ($\tilde{\dot{\varepsilon}}_m$) and predicted ($\hat{\dot{\varepsilon}}_m$) minimum strain rates.

lower-stress conditions [28,29].

To account for the tertiary creep regime, Kachanov and Rabotnov proposed interfacing the Continuum Damage Mechanics (CDM) framework with Norton's power law [16]. This leads to a set of creep damage constitutive equations:

$$\dot{\varepsilon} = \frac{d\varepsilon}{dt} = A\left(\frac{\sigma}{1-\omega}\right)^n \tag{2}$$

$$\dot{\omega} = \frac{d\omega}{dt} = \frac{M\sigma^\chi}{(1-\omega)^\varphi} \tag{3}$$

where ω is the creep damage, A and n are the Norton's power law material parameters from Eq. (1), while M, φ, and χ are material parameters describing the tertiary creep region. It is assumed that the stress and temperature are constant. The initial conditions are set such that $t_0 = 0$ and $\omega_0 = 0$, where t_0 represents the initial time and ω_0 represents the initial damage. With these assumptions, the damage evolution equation (Eq. (3)) can be integrated and simplified as follows:

$$\int_{\omega_0=0}^{\omega} (1-\omega)^\varphi d\omega = \int_{t_0=0}^{t} M\sigma^\chi dt \tag{4}$$

$$\omega = 1 - [1 - (\varphi+1)M\sigma^\chi t]^{\frac{1}{\varphi+1}} \tag{5}$$

The creep damage expression in Eq. (5) can then be substituted into the creep damage constitutive equation proposed by Kachanov and Rabotnov (Eq. (2)) to eliminate the creep damage variable:

$$\dot{\varepsilon} = \frac{d\varepsilon}{dt} = A\left(\frac{\sigma}{[1-(\varphi+1)M\sigma^\chi t]^{\frac{1}{\varphi+1}}}\right)^n \tag{6}$$

This expression can be integrated with the assumption that $\varepsilon_0 = \hat{\varepsilon}_0$,

where ε_0 represents the initial creep strain, and $\hat{\varepsilon}_0$ is the predicted strain offset to account for the primary creep, as follows:

$$\int_{\varepsilon_0=\hat{\varepsilon}_0}^{\varepsilon} d\varepsilon = A\sigma^n \int_{t_0=0}^{t} [1-(\varphi+1)M\sigma^\chi t]^{-\frac{n}{\varphi+1}}dt \tag{7}$$

The resulting expression in Eq. (8) defines the form of the K-R model used in the present work, which describes the creep strain as a function of time and five temperature-dependent material parameters (A, n, M, φ, and χ).

$$\varepsilon(t) = A\sigma^n \frac{[1-(\varphi+1)M\sigma^\chi t]^{\frac{\varphi+1-n}{\varphi+1}} - 1}{M\sigma^\chi(n-\varphi-1)} + \hat{\varepsilon}_0 \tag{8}$$

The challenge of the K-R model lies in finding these five unknown material parameters, which describe the creep behaviour of the alloy at various stress conditions. As described in Refs. [16,17], the general approach is to first determine the A and n parameters by linearising Norton's power law (Eq. (1)) and applying linear regression (see Appendix B). Once the A and n parameters have been computed, the M, φ, and χ parameters are obtained using trial-and-error approaches or an optimisation algorithm. Our study presents an alternative approach whereby the MOGA will be used to simultaneously optimise all five material parameters.

4. Multi-objective genetic algorithm (MOGA)

Here, we employed the MOGA implementation from the PYMOO library [34] for computing the values of all five unknown material parameters (A, n, M, φ, and χ) defining the K-R creep model (Eq. (8)). In short, all genetic algorithms (GA) are based on a randomised search technique inspired by the principles of natural selection, and thus use terminology related to genetics such as *gene*, *chromosomes*, *population*, *mating*, *crossover*, and *mutation rate* [35–37]. In the context of the outlined optimisation problem, a *gene* is a scalar representing one of the unknown material parameters (A, n, M, φ, or χ), a *chromosome* is an array representing a set of these material parameters ($[A, n, M, \varphi, \chi]$), and a *population* represents a collection of *chromosomes* (i.e., the material parameter set used in the K-R model). The objective of the GA optimiser is then to produce a *population* of *chromosomes*, which best satisfy one or multiple objective functions, thus finding a set of five material parameters, which lead to the most accurate K-R model prediction when compared to the observed elevated-temperature material behaviour.

The GA begins with an initial population containing chromosomes with randomly generated genes. The GA iteratively improves the population by selectively breeding the chromosomes every generation. The selection process for the breeding involves evaluating the fitness of each chromosome against one or multiple objective functions, whereby chromosomes with higher fitness levels will be chosen to breed and thus pass on their genetic information to their offspring. The breeding of chromosome pairs relies mainly on the so-called crossover and mutation operations. The crossover operation involves swapping the genes between two chromosomes to produce an offspring. The mutation operation involves randomly changing one or more genes in the offspring, to promote diversity as the population evolves, and thus avoid a local minimum solution.

In implementing the MOGA, the user must define appropriate values for the hyperparameters to ensure the optimal performance of the MOGA. These hyperparameters include the crossover probability, mutation probability, initial population, and number of offspring. Here, these parameters were respectively set to 65%, 35%, 800, and 800. These values were the result of an extensive parametric sensitivity study, as detailed in Appendix A.

In addition to defining the hyperparameter values, the user must also specify the bounds for the material parameters (A, n, M, φ, and χ), to define the shape of the parameter search space. The initial values for the

lower and upper bounds were based on literature [16,17]. Through trial-and-error, the final set of lower and upper bounds were set to the values shown in Table 1. This final set of bounds was selected such that the search space was small enough that the MOGA could converge in a reasonable amount of time, but large enough to showcase the MOGA's optimisation capabilities.

Finally, we configured the MOGA to evaluate the fitness of individual chromosomes in the population by assessing the performance of the K-R model creep curve predictions against the experimental creep curves, using four objective functions. These objective functions measure the deviations between the K-R model predictions and the experimental data using the mean square errors defined as:

$$E_\varepsilon(A,n,M,\varphi,\chi) = \frac{1}{S_1}\sum_{i=1}^{S_1}\frac{1}{S_2}\sum_{j=1}^{S_2}\left((\widetilde{\varepsilon})_{i,j} - (\widehat{\varepsilon})_{i,j}\right)^2 = \frac{1}{S_1}\sum_{i=1}^{S_1}\frac{1}{S_2}\sum_{j=1}^{S_2}\left((\widetilde{\varepsilon})_{i,j} - \left(A(\sigma_{i,j})^n\frac{\left[1 - (\varphi+1)M(\sigma_{i,j})^\chi t_{i,j}\right]^{\frac{\varphi+1-n}{\varphi+1}} - 1}{M(\sigma_{i,j})^\chi(n-\varphi-1)} + (\widehat{\varepsilon}_0)_i\right)\right)^2 \tag{9}$$

$$E_{t_f}(M,\varphi,\chi) = \frac{1}{S_1}\sum_{i=1}^{S_1}\left((\widetilde{t_f})_i - (\widehat{t_f})_i\right)^2 = \frac{1}{S_1}\sum_{i=1}^{S_1}\left((\widetilde{t_f})_i - \frac{1}{(\varphi+1)M(\sigma_i)^\chi}\right)^2 \tag{10}$$

$$E_{\varepsilon_f}(A,n,M,\varphi,\chi) = \frac{1}{S_1}\sum_{i=1}^{S_1}\left((\widetilde{\varepsilon}_f)_i - (\widehat{\varepsilon}_f)_i\right)^2 = \frac{1}{S_1}\sum_{i=1}^{S_1}\left((\widetilde{\varepsilon}_f)_i - \left(\frac{A(\sigma_i)^n}{M(\sigma_i)^\chi(\varphi+1-n)} + (\widehat{\varepsilon}_0)_i\right)\right)^2 \tag{11}$$

$$E_{\dot{\varepsilon}_m}(A,n) = \frac{1}{S_1}\sum_{i=1}^{S_1}\left((\widetilde{\dot{\varepsilon}}_m)_i - (\widehat{\dot{\varepsilon}}_m)_i\right)^2 = \frac{1}{S_1}\sum_{i=1}^{S_1}\left((\widetilde{\dot{\varepsilon}}_m)_i - A(\sigma_i)^n\right)^2 \tag{12}$$

where S_1 represents the number of experimental datasets used in the optimisation process, and S_2 represents the size of each experimental dataset – here, $S_2 = 50$, as explained in section 2. The individual objective functions are described below and represented schematically in Fig. 2.

(1) E_ε (Eq. (9)) evaluates the mean square error between all 50 creep strain values on the predicted ($\widehat{\varepsilon}$) and experimentally observed ($\widetilde{\varepsilon}$) creep curves (excluding the primary creep), for each dataset. Minimising E_ε will effectively minimise the common area between the predicted and experimental curves – i.e., the shaded

area, Ω, in Fig. 2. Thus, for each creep curve, as $E_\varepsilon \rightarrow 0$, $\Omega =$

$\int_{t_p}^{\widehat{t_f}}\widehat{\varepsilon}dt - \int_{t_p}^{\widetilde{t_f}}\widetilde{\varepsilon}dt \rightarrow 0$, where t_p represents the time in which the primary creep regime ends.

(2) E_{t_f} (Eq. (10)) evaluates the mean square error between the predicted time-to-failure ($\widehat{t_f}$) and the experimentally observed time-to-failure ($\widetilde{t_f}$), for each dataset. Minimising E_{t_f} will effectively minimise the horizontal displacement between the endpoints of the predicted and experimental curves – i.e., the difference between the $\widehat{t_f}$ and $\widetilde{t_f}$ values. Thus, for each creep curve, as $E_{t_f} \rightarrow 0$, $\widehat{t_f} - \widetilde{t_f} \rightarrow 0$.

(3) E_{ε_f} (Eq. (11)) evaluates the mean square error between the predicted strain-to-failure ($\widehat{\varepsilon}_f$) and the experimentally observed strain-to-failure ($\widetilde{\varepsilon}_f$), for each dataset. Minimising E_{ε_f} will effectively minimise the vertical displacement between the endpoints of the predicted and experimental curves – i.e., the difference between the $\widehat{\varepsilon}_f$ and $\widetilde{\varepsilon}_f$ values. Thus, for each creep curve, this means that as $E_{\varepsilon_f} \rightarrow 0$, $\widehat{\varepsilon}_f - \widetilde{\varepsilon}_f \rightarrow 0$.

(4) $E_{\dot{\varepsilon}_m}$ (Eq. (12)) evaluates the mean square error between the predicted minimum creep rate ($\widehat{\dot{\varepsilon}}_m$) and the experimentally observed minimum creep rate ($\widetilde{\dot{\varepsilon}}_m$), for each dataset. As $\dot{\varepsilon}_m$ represents the slope of the creep curve in the secondary creep stage, minimising $E_{\dot{\varepsilon}_m}$ will approximate the alignment between the observed and the predicted creep curves in the secondary region. For each creep curve, as $E_{\dot{\varepsilon}_m} \rightarrow 0$, $\widehat{\dot{\varepsilon}}_m - \widetilde{\dot{\varepsilon}}_m \rightarrow 0$. Note that even in the case of perfect alignment ($\widehat{\dot{\varepsilon}}_m = \widetilde{\dot{\varepsilon}}_m$) the creep curves might be offset (parallel) from each other, with this offset being the difference between the observed and predicted primary creep strain ($\widehat{\varepsilon}_p - \widetilde{\varepsilon}_p$).

By means of these four predefined objective functions, the MOGA promotes solutions that lead to the smallest discrepancy (error) between the K-R model creep curve predictions (Eq. (8)) and INL's experimental creep curves. In other words, only chromosomes leading to small deviations of the K-R model from the experimental data are allowed to propagate so that the final population of chromosomes contains a large number of good solutions. We selected the optimal chromosome (i.e., the set of the five material parameters) from the final population by checking which chromosome best satisfied all four objective functions (Eq. (9) - (12)). This was done by summing the normalised mean square error values for the four objective functions, in which the optimal set of material parameter (A, n, M, φ, and χ) values gave the minimum value for the total normalised mean square error. This is expressed mathematically in Eq. (13), where $\overline{\widetilde{\varepsilon}}$, $\overline{\widetilde{t_f}}$, $\overline{\widetilde{\varepsilon}_f}$, and $\overline{\widetilde{\dot{\varepsilon}}_m}$ are the average values of the experimental strain, time-to-failure, strain-to-failure, and minimum creep rate.

Table 1
Lower and upper bounds of the material parameters of the K-R model.

	A	n	M	φ	χ
Lower Bound	10^{-20}	0	0	0	0
Upper Bound	10^{-5}	10^1	10^0	10^2	10^1

$$A, n, M, \varphi, \chi = \underset{A,n,M,\varphi,\chi}{\arg\min} \left\{ w_\varepsilon \frac{\sqrt{E_\varepsilon}}{\overline{\overline{\varepsilon}}} + w_{t_f} \frac{\sqrt{E_{t_f}}}{\overline{\overline{t}}_f} + w_{\varepsilon_f} \frac{\sqrt{E_{\varepsilon_f}}}{\overline{\overline{\varepsilon}}_f} + w_{\dot{\varepsilon}_m} \frac{\sqrt{E_{\dot{\varepsilon}_m}}}{\overline{\overline{\dot{\varepsilon}}}_m} \right\} \qquad (13)$$

The weights, w_ε, w_{t_f}, w_{ε_f}, and $w_{\dot{\varepsilon}_m}$, are specified by the user to be equal to 1, which puts equal weighting on all four normalised mean square errors. This is because the aim was to predict the full creep curves as accurately as possible, and thus evaluate the K-R model's performance in capturing the overall creep behaviour of the studied alloy.

However, if desired, an analyst can prioritise minimising a specific error by introducing uneven weights in Eq. (13). For example, the time-to-failure (t_f) is typically of the highest priority for most engineering applications, so one could increase the weight, w_{t_f}, associated with the E_{t_f} objective function. Note that it is not recommended to set one of the weights to zero. Since each source of error serves a purpose in the optimisation process, negating one of them can result in abnormally shaped predictions.
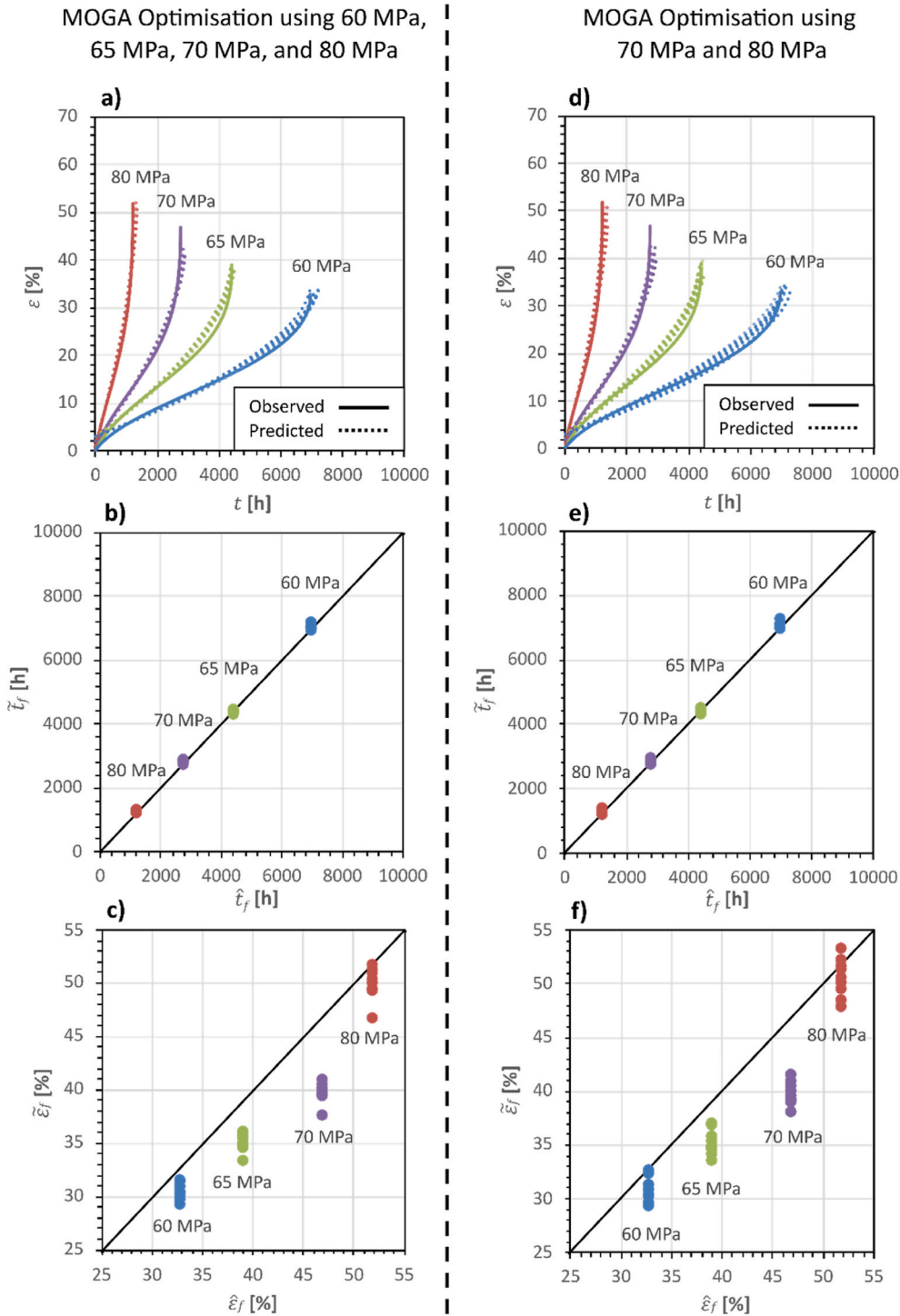
Fig. 3. Results of the optimisation at 800 °C with all stress conditions (approach 1, at 60*MPa*, 65*MPa*, 70*MPa*, and 80*MPa*) on the left, and limited stress conditions (approach 2, at 70*MPa* and 80*MPa*) on the right. Plots in a) and d) display the observed (solid) and predicted (dotted) creep curves. Plots in b) and e) display the observed and predicted times-to-failure. Plots in c) and f) display the observed and predicted strains-to-failure.

5. Results and discussion

In what follows, we first validate the proposed methodology by predicting the creep behaviour of Alloy 617 at 800°C. We then evaluate the accuracy of the K-R creep model predictions by direct comparison with the experimentally measured time- and strain-to failure (t_f, ε_f), as these hold the most value in elevated-temperature engineering applications. We also pay attention to the prediction of the kinetics of the creep plasticity – i.e., the ability of the utilised K-R model to capture the shape of the measured creep curves. Finally, we employ the validated methodology in predicting the creep behaviour of the studied alloy at 900°C and 1000°C at various stress conditions.

5.1. Predicting creep of alloy 617 at 800°C

To test the robustness of the proposed methodology (i.e., coupled K-R model and MOGA optimisation), we performed the MOGA optimisation with the INL produced experimental data (Fig. 1) using two different approaches:

(1) Firstly, the MOGA optimisation of the five K-R model's (Eq. (8)) material parameters was performed by trying to satisfy the pre-defined objective functions (E_ε, E_{t_f}, E_{ε_f}, and $E_{\dot{\varepsilon}_m}$) for all available experimental creep curves at the given temperature (60MPa, 65MPa, 70MPa, and 80MPa, at 800°C, Fig. 1a). Hence, $S_1 = 4$ in the objective function expressions defined in Eqs. (9)–(12).

(2) Secondly, the MOGA optimisation of the five K-R model's (Eq. (8)) material parameters was performed by trying to satisfy the pre-defined objective functions (E_ε, E_{t_f}, E_{ε_f}, and $E_{\dot{\varepsilon}_m}$) only for the short-term creep experimental data (70MPa and 80MPa). Hence, $S_1 = 2$ in the definitions for the objective function shown in Eqs. (9)–(12) – this is because this approach uses only 2 available experimental creep curves to find an optimal set of K-R model's (Eq. (8)) material parameters. The long-term creep experimental data (60MPa and 65MPa) are later used to validate the accuracy of the K-R creep model in extrapolating to longer lifetimes than the model training data (i.e., to predict the experimental data that was not used in the optimisation of the model's parameters).

Note that a MOGA optimisation conducted with all stress conditions (approach 1) took an average of 4600 s of CPU time on a 3.80 GHz Intel Core i7-10700KF processor. A MOGA optimisation with limited stress conditions (approach 2) took approximately half that time, due to the process computing half the calculations. We summarise the results for ten repeat optimisations using both approaches in Fig. 3, where the plots on the left (Fig. 3a–c) are from the first approach, and the plots on the right (Fig. 3d–f) are from the second approach.

The plot in Fig. 3a compares the observed and predicted creep curves when the MOGA optimisations were conducted by taking into the account all experimental data (approach 1). It becomes clear when comparing the experimental and predicted creep curves that the MOGA optimiser can consistently find a good set (chromosome) of material parameters (A, n, M, φ, and χ) for the K-R creep model, which can then capture the overall elevated-temperature behaviour of the alloy. In particular, the K-R model is very accurate when it comes to predicting the time-to-failure (t_f). This is evident from Fig. 3b, which compares the predicted and observed t_f – notice that all the predictions are on the 1:1 line. While the K-R model is not as accurate in predicting the strain-to failure (ε_f), as seen in see Fig. 3c, the predictions are conservative and can be thus considered 'acceptable' from an engineering application perspective. When it comes to the predictions of the kinetics of the creep plasticity, one can see in Fig. 3a that the model captures the overall creep behaviour reasonably well. Specifically, the predicted creep curve aligns well with the experimental curve in the secondary creep regime; this indicates that the minimum creep rate is a good representation of

the secondary creep regime for Alloy 617. However, the K-R model's predictions seem to show a less distinctive secondary-to-tertiary transition. Recall that here we are considering only the secondary and tertiary creep regions (Fig. 3), as the K-R creep model does not account for the primary creep (see section 2), and in general Alloy 617 exhibits only limited primary creep [28,29].

Fig. 3d–f presents the results of the MOGA optimisations conducted using the short-term experimental creep curves at 70MPa and 80MPa (approach 2). In other words, the MOGA optimisation searches for the material parameters of K-R model by attempting to satisfy only the short-term creep measurements (creep curves). The MOGA-identified K-R model's material parameters (A, n, M, φ, and χ) were then used to predict the long-term creep behaviour at the lower stress conditions (60MPa and 65MPa) as well as higher stress conditions (70MPa and 80MPa). As it can be seen in Fig. 3d, the accuracy of the employed methodology did not suffer when we limited the experimental data in the MOGA optimisation only to the short-term creep curves (i.e., high stress conditions). The time-to-failure (t_f) is again predicted with a high accuracy (Fig. 3e), with all the predictions along the 1:1 line. Like the results from the first approach shown in Fig. 3c, the predictions of the strain-to-failure (ε_f) using the second approach shown in Fig. 3e are not as accurate as the t_f predictions. However, the ε_f predictions are again mostly conservative, which is considered 'acceptable' from an engineering perspective. Lastly, when it comes to the prediction of the kinetics of the creep plasticity, the K-R model again predicts a less distinctive secondary-to-tertiary transition when compared to the experimental measurements. However, it captures the overall secondary and tertiary creep regime behaviour of the Alloy 617 reasonably well.

Hence, it is concluded that the K-R creep model can accurately capture the creep behaviour of Alloy 617, and that the MOGA performs well when searching for the unknown material parameters in a large parameter space (Table 1). Moreover, the K-R model paired with the MOGA is capable of predicting the long-term creep behaviour of Alloy 617 from shorter term data even when the long-term experimental data is not available. Specifically, it is shown that two sets of short-term creep experimental data are sufficient to fully optimise the K-R creep model using the MOGA methodology. This is of technological significance, as in practice, it is easier and less costly to obtain the short-term experimental data (at higher stress conditions) than the long-term experimental data (at lower stress conditions), which are typically found in the operational conditions of many elevated-temperature systems. Furthermore, these results point to the thermal stability of the microstructure of Alloy 617 at 800°C – i.e., the alloy has a consistent creep mechanism at the various stress conditions. However, caution is recommended if applying this approach at the lower temperature of 750°C, which coincides with the formation of γ' precipitates [38], whereby there is a change of creep mechanism to a threshold stress behaviour [29].

Next we briefly discuss the repeatability of the MOGA optimisation, which is inherently connected to the accuracy of the K-R creep model predictions. Due to the random nature of MOGA optimisation, finding a unique and reproducible result is not guaranteed. One thus needs to look into the reproducibility and consistency of finding an optimal solution (chromosome) – in our case, an optimal set of stress-independent K-R model's material parameters (A, n, M, φ, and χ), which best describes the observed creep data. We utilised boxplots to analyse the material parameter values obtained from the two approaches defined above – these boxplots can be seen in Fig. 4. To better analyse the statistical variability, an additional 40 optimisations were conducted for each approach (in addition to the 10 shown in Fig. 3). It is clear from Fig. 4 that there is a measurable variation in the values of the searched material parameters identified in the 50 independent MOGA optimisations. However, it is also clear that the MOGA can identify the searched material parameters consistently within a reasonable limit. The maximum, minimum, average, and standard deviations of the determined material parameters for both approaches are tabulated in Table 2 and Table 3.
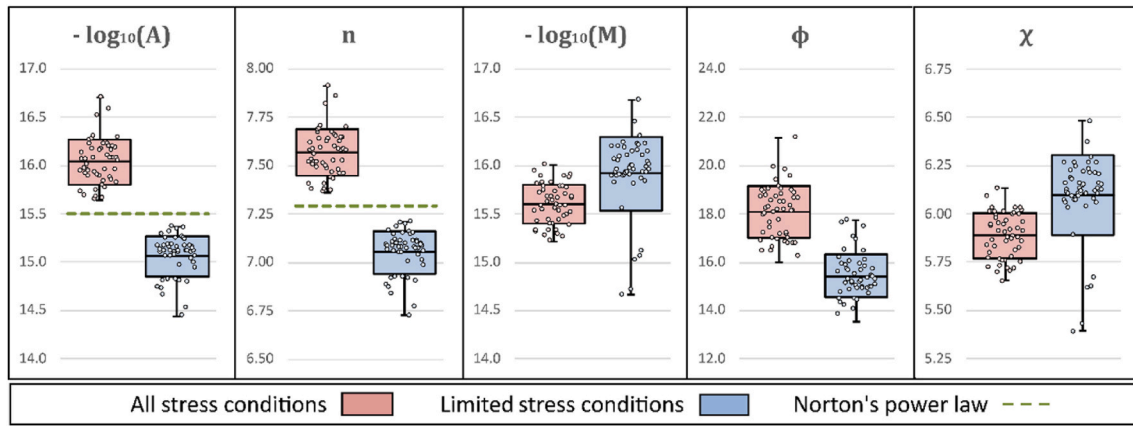
Fig. 4. Boxplots of optimised material parameters of the K-R model (A, n, M, φ, and χ) at 800 °C for all stress conditions (approach 1, at $60MPa$, $65MPa$, $70MPa$, and $80MPa$) on the left (red), and limited stress conditions (approach 2, at $70MPa$ and $80MPa$) on the right (blue). In the boxplots, the horizontal lines represent the mean, the boxes represent the standard deviations, and the whiskers represent the range. The green dotted lines represent the values of the A and n parameters obtained from Norton's power law. (For interpretation of the references to colour in this figure legend, the reader is referred to the Web version of this article.)

Table 2
Summary of the MOGA optimisations at 800 °C for all stress conditions ($60MPa$, $65MPa$, $70MPa$, and $80MPa$).

	Approach 1				
	A	n	M	φ	χ
Maximum	2.51×10^{-16}	7.91	6.31×10^{-16}	21.2	6.14
Minimum	2.00×10^{-17}	7.36	1.00×10^{-16}	16.2	5.65
Average	1.00×10^{-16}	7.57	2.51×10^{-16}	18.1	5.89
Standard Deviation	0.587	0.121	0.625	1.06	0.117

Table 3
Summary of the MOGA optimisations at 800°C for limited stress conditions ($70~MPa$ and $80~MPa$).

	Approach 2				
	A	n	M	ϕ	χ
Maximum	3.98×10^{-16}	7.21	2.00×10^{-17}	17.8	6.48
Minimum	3.98×10^{-15}	6.73	2.00×10^{-15}	13.8	5.39
Average	7.94×10^{-16}	7.05	1.2610^{-16}	15.4	6.10
Standard Deviation	0.622	0.108	0.412	0.886	0.210

Both approaches yielded similar results, which points to the microstructural stability of Alloy 617 and the ability of K-R model to capture its creep behaviour. However, when examining the material parameter values in Fig. 4, the most noticeable difference is with identifying the A and n parameters – these define the secondary creep regime via Norton's power law (Eq. (1)). When using the first approach, A and n have average values of 1.00×10^{-16} and 7.57 (red/left-hand side boxplots in Fig. 4). When using the second approach, A and n have average values of 7.94×10^{-16} and 7.05 (blue/right-hand side boxplots in Fig. 4). Finally, when obtaining the A and n parameters from the linearisation of Norton's power law (see Appendix B), A and n had values of 3.15×10^{-16} and 7.29 (green dashed lines in Fig. 4). While both approaches produced A and n values close to those obtained from Norton's power law, neither approach can be considered more accurate than the other. The first approach yields A and n values higher than those identified by the power law, while the second approach yields lower values. When it comes to finding the M, φ, and χ material parameters, which define the tertiary creep regime (Eq. (3)), both approaches lead to very similar results with a significant overlap in the identified solutions. However, when using only two short-term creep curves for the model optimisation (approach 2), there is a greater spread in the identified M, φ, and χ material parameters from the 50 independent MOGA optimisation runs. This is

likely due to the fact that having two creep curves in the MOGA optimisation (approach 2) constrains the MOGA optimisation solution space to a lesser degree than when we use all available experimental data (approach 1).

5.2. Predicting creep of alloy 617 at $900°C$ and $1000°C$

After demonstrating that coupling the K-R model with MOGA optimisation yields satisfactory results at 800 °C, we attempted the same methodology to predict the creep behaviour of Alloy 617 at $900°C$ and $1000°C$ (Figs. 1 and 2). As such, we again conducted ten independent optimisations utilising the available INL-produced experimental data while adopting the two approaches defined above. This was done independently at both temperatures because we are using the temperature-independent implementation of the K-R creep model (Eq. (8)). The obtained predictions are then compared with the experimental data in Fig. 5 (900°C) and Fig. 6 (1000°C). The results of the first optimisation approach (utilising all available experimental data) are again on the left, and the results of the second optimisation approach (utilising only the short-term experimental data) are again on the right.

While the creep predictions at 900°C (Fig. 5) are more accurate than those at 1000°C (Fig. 6), the predictions at both temperatures are significantly less accurate when compared to the predictions obtained at 800°C (Fig. 3 in section 5.1). Furthermore, as it can be seen in Figs. 5 and 6, predictions at these temperatures vary significantly. The decreased accuracy and consistency in the creep predictions indicate a change in the ongoing creep mechanism, which is thought to be triggered by oxidation at these higher temperatures, which has been found to be significant when testing Alloy 617 in air [30–32]. As it is evident from Fig. 1b–c, the cumulative effect of oxidation over the relatively longer creep lives results in unconventional creep behaviour, which manifests itself by atypically shaped creep curves. Since the oxidation is a diffusion-controlled process, the shorter tests are inherently less affected. In other words, the effect of oxidation becomes more pronounced in the long-term creep tests ($> 5000h$) that were conducted at lower stress conditions (i.e., 900°C /26 MPa, 1000°C /11 MPa, 1000°C /12 MPa, and 1000°C /13 MPa). Thus, the K-R creep model's inability to account for the shift in creep behaviour over long times at very high temperatures, resulted in the decreased accuracy in the creep predictions at 900°C and 1000°C.

It can also be observed that, at both 900°C and 1000°C, the creep predictions using approach 1 (utilising all available data) is less accurate and has a greater variance, when compared to the creep predictions using approach 2 (utilising only short-term data). This can be attributed to the fact that approach 1 includes the long-term creep tests in the
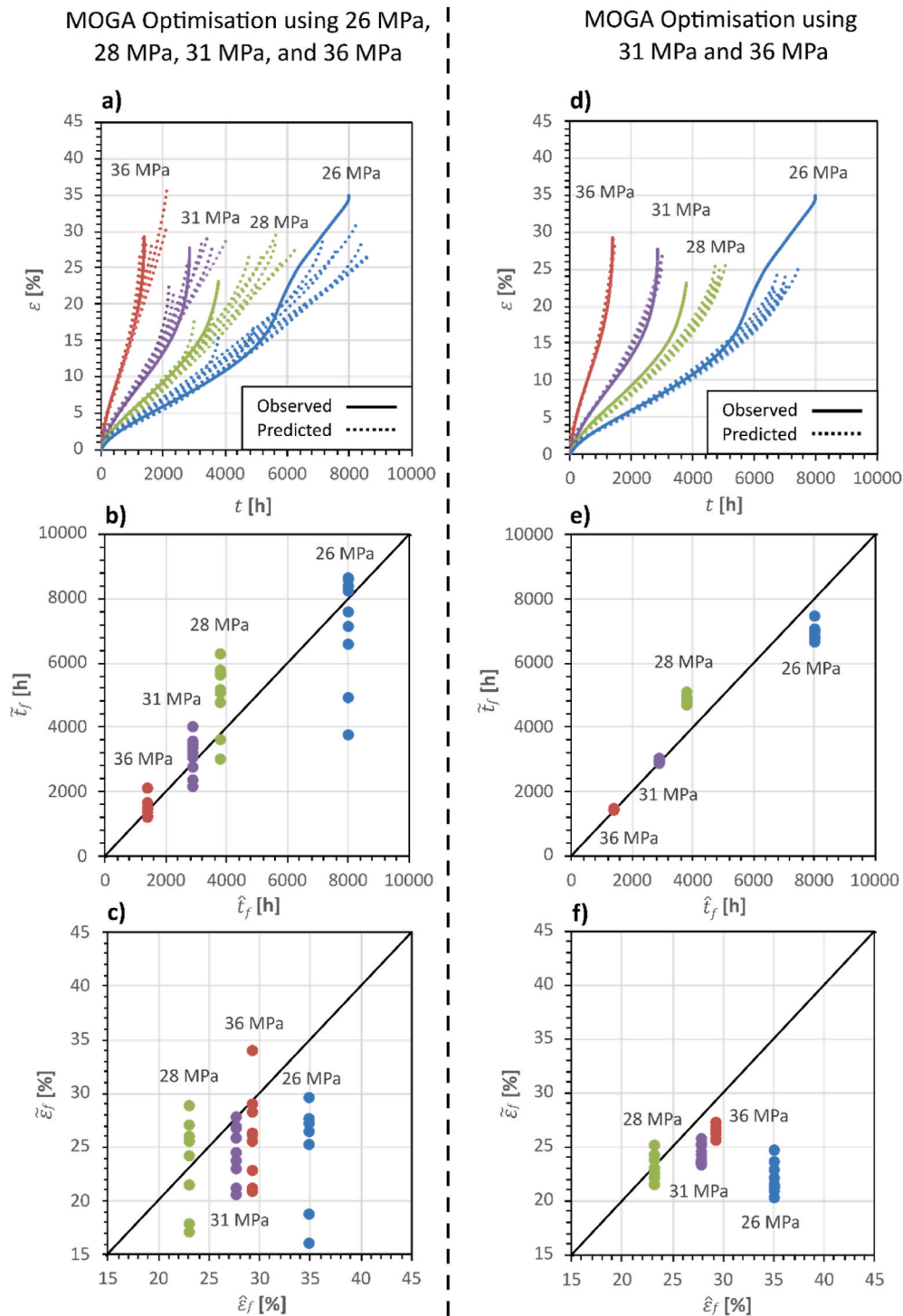
Fig. 5. Results of the optimisation at 900 °C with all stress conditions (approach 1, at 26*MPa*, 28*MPa*, 31*MPa*, and 36*MPa*) on the left, and limited stress conditions (approach 2, at 31*MPa* and 36*MPa*) on the right. Plots in a) and d) display the observed (solid) and predicted (dotted) creep curves. Plots in b) and e) display the observed and predicted times-to-failure. Plots in c) and f) display the observed and predicted strains-to-failure.

MOGA optimisation, while approach 2 excludes them. The atypically shaped creep curves cannot be accounted for by the K-R creep model (Eq. (8)), nor by the associated MOGA objective functions (Eq. (9) - (12)). As such, their inclusion in the optimisation severely compromised the performance of the MOGA by introducing regions of false minima in the optimisation space.

Nevertheless, the proposed methodology utilising the MOGA does work within the limits of the employed K-R creep model. As shown in Figs. 5 and 6, the model can provide indicative results when it comes to

the t_f and ε_f predictions at both temperatures. It is, however, recommended that the analyst wishing to optimise the K-R model using MOGA optimisation checks the repeatability and consistency of the solution to avoid solution outliers.

6. Conclusion

In this study, we introduced the methodology of combining the temperature-dependent Kachanov-Rabotnov (K-R) creep model with

Fig. 6. Results of the optimisation at 1000 °C with all stress conditions (approach 1, at 11*MPa*, 12*MPa*, 13*MPa*, and 16*MPa*) on the left, and limited stress conditions (approach 2, at 13*MPa* and 16*MPa*) on the right. Plots in **a)** and **d)** display the observed (solid) and predicted (dotted) creep curves. Plots in **b)** and **e)** display the observed and predicted times-to-failure. Plots in **c)** and **f)** display the observed and predicted strains-to-failure.
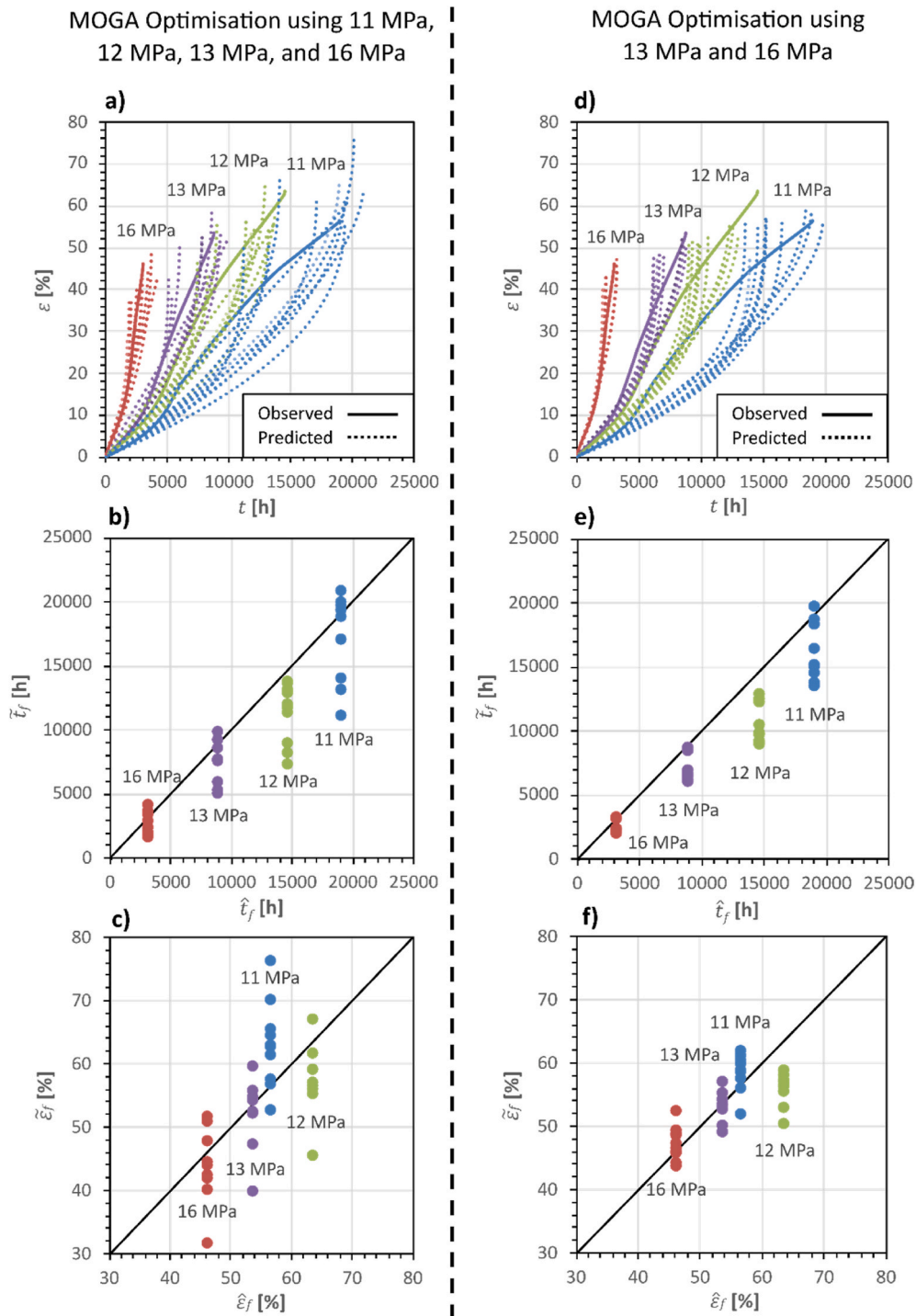
multi-objective genetic algorithm (MOGA) optimisation. We evaluated the methodology against the experimental data for the prediction of creep behaviour of Alloy 617 at 800°C, 900°C, and 1000°C, under various stress conditions.

We demonstrated that the K-R model was capable of capturing the elevated-temperature behaviour of Alloy 617 at 800°C under a wide range of stress conditions, even when the model was optimised utilising limited experimental data (short-term creep curves). In particular, the MOGA-optimised K-R creep model was able to predict the time-to-

failure (t_f) with excellent accuracy. While the strain-to-failure (ε_f) predictions are not as accurate, they are generally conservative, even though the predictions' conservatism is not guaranteed. The overall behaviour (i.e., the kinetics of the creep plasticity accumulation) of the alloy at 800°C is also reasonably well captured, even though the prediction of the secondary-to-tertiary creep regime transition is somewhat less distinct when compared to the experimental data.

We also investigated the performance of the methodology with creep data at 900°C and 1000°C. The accuracy of the K-R model predictions

dropped significantly when trying to capture the behaviour of Alloy 617 at those temperatures, especially for the creep data obtained at low stress conditions. This was attributed to oxidation, which affects the accumulation of the creep strain and the failure mechanism, resulting in an atypical creep curve shape that the K-R model cannot capture. Due to the diffusion characteristic of the oxidation process, this has more pronounced effect in the case of long-term creep tests (i.e., low stresses). As such, the kinetics of the creep plasticity during the long-term creep tests is not well captured. Nevertheless, we have shown that MOGA-optimised K-R models can still provide an indicative result when it comes to the time-to-failure (t_f), and strain-to-failure (ε_f) predictions at the higher temperatures. Additionally, based on our repeated runs of up to 50 optimisations, it is recommended that at least 10 independent MOGA optimisations should be conducted to ensure the repeatability and consistency of the solution. This becomes particularly important when trying to optimise the K-R model under conditions where creep mechanism changes from oxidation and/or microstructure evolution might occur.

Ultimately, we have demonstrated that MOGA optimisation can consistently find a set of stress-independent material parameters (A, n, M, φ, and χ) for the K-R creep model, which can provide accurate secondary and tertiary creep predictions, when the creep mechanism remains constant. Future advancements could involve employing microstructure-informed creep models, such as crystal-plasticity models, to predict all three stages of elevated-temperature creep behaviour. However, the evaluation of such models is often computationally expensive, which introduces additional challenges regarding the optimisation of the material parameters.

Author statement

J. Choi: Investigation, Software, Formal analysis, Methodology, Visualization, Writing - Original Draft, **L. Bortolan Neto**: Methodology, Supervision, Writing - Review & Editing, **R. N. Wright**: Resources, **J. J. Kruzic**: Supervision, Writing - Review & Editing, **O. Muránsky**: Conceptualization, Methodology, Visualization, Writing - Original Draft, Supervision, Project administration.

Declaration of competing interest

The authors declare that they have no known competing financial interests or personal relationships that could have appeared to influence the work reported in this paper.

Data availability

Data will be made available on request.

Appendix C. Supplementary data

Supplementary data to this article can be found online at https://doi.org/10.1016/j.ijpvp.2022.104721.

Appendix A

The performance of the MOGA is heavily dependent on the user-defined values for the hyperparameters, namely the crossover probability, mutation probability, initial population, and number of offspring. The values of these hyperparameters vary for different optimisation problems. Thus, to determine appropriate hyperparameter values for the parameter optimisation of the K-R creep model, we conducted a sensitivity study using the INL creep data at $60 MPa$, $65 MPa$, $70 MPa$, and $80 MPa$, at $800°C$.

The results of the study are in the form of two heatmaps (Fig. A1) and a plot (Fig. A2), which use the total normalised mean square error values of the four objective functions, as seen in Eq. (13). The first heatmap studies the crossover probability and mutation probability pairs, in which an appropriate pair was found to be 65% and 35%, respectively. The second heatmap studies the initial population and number of offspring pairs, in which an appropriate pair was found to be 800 and 800, respectively. Using these hyperparameter values, the plot studies the number of generations required to reach the steady-state value for the total normalised error, which was found to be approximately 4000 generations. For each pair in the heatmaps and value in the plots, the MOGA was used to conduct 5 optimisations on the A, n, M, φ, and χ parameters. This was done to improve the reliability of the results.

a)

Crossover Probability (%)

Mutation Probability (%)	50	55	60	65	70	75	80	85	90	95
5	0.8	1.02	0.85	0.91	0.28	0.83	0.72	0.98	1.02	0.92
10	0.51	0.75	0.98	0.82	0.67	0.5	0.96	0.29	0.78	1.07
15	0.33	0.27	0.3	0.51	0.5	0.71	0.54	0.56	1.02	0.64
20	0.28	0.29	0.29	0.51	0.35	0.43	0.53	0.67	0.31	0.69
25	0.23	0.43	0.3	0.45	0.45	0.36	0.48	0.35	0.43	0.5
30	0.31	0.28	0.28	0.3	0.33	0.29	0.29	0.35	0.36	0.37
35	0.3	0.26	0.25	0.28	0.27	0.28	0.27	0.29	0.3	0.4
40	0.31	0.34	0.25	0.26	0.32	0.29	0.33	0.32	0.31	0.41
45	0.35	0.24	0.32	0.34	0.32	0.33	0.29	0.32	0.26	0.32
50	0.26	0.25	0.25	0.26	0.3	0.36	0.28	0.35	0.41	0.27

b)

Initial Population

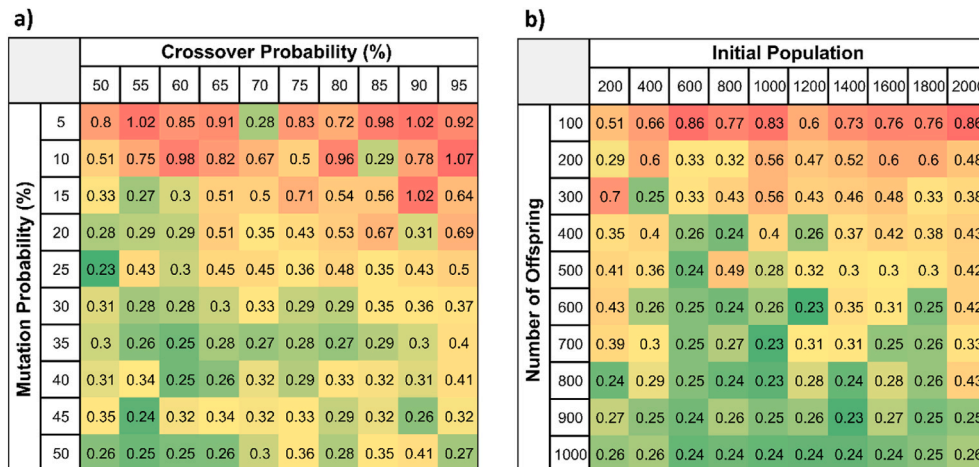| Number of Offspring	200	400	600	800	1000	1200	1400	1600	1800	2000
100	0.51	0.66	0.86	0.77	0.83	0.6	0.73	0.76	0.76	0.86
200	0.29	0.6	0.33	0.32	0.56	0.47	0.52	0.6	0.6	0.48
300	0.7	0.25	0.33	0.43	0.56	0.43	0.46	0.48	0.33	0.38
400	0.35	0.4	0.26	0.24	0.4	0.26	0.37	0.42	0.38	0.43
500	0.41	0.36	0.24	0.49	0.28	0.32	0.3	0.3	0.3	0.42
600	0.43	0.26	0.25	0.24	0.26	0.23	0.35	0.31	0.25	0.42
700	0.39	0.3	0.25	0.27	0.23	0.31	0.31	0.25	0.26	0.33
800	0.24	0.29	0.25	0.24	0.23	0.28	0.24	0.28	0.26	0.43
900	0.27	0.25	0.24	0.26	0.25	0.26	0.23	0.27	0.25	0.25
1000	0.26	0.26	0.24	0.24	0.24	0.24	0.24	0.24	0.25	0.26

Fig. A1. The heatmaps in a) and b) plot the crossover probability against the mutation probability, and the initial population against the number of offspring, respectively. Each cell represents the averaged total normalised error (Eq. (13)) of 5 optimisations at 800 °C.
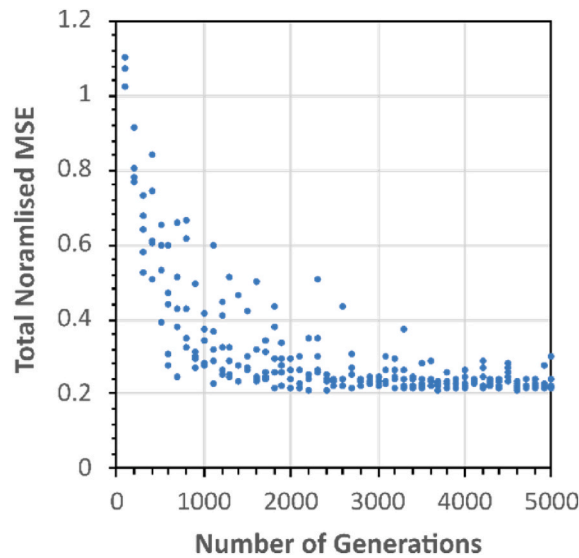
Fig. A2. Plot of the total normalised error (Eq. (13)) against the number of generations at 800 ° C.

Appendix B

Norton's power law can be linearised by wrapping both sides of the expression in Eq. (1) by the natural logarithmic function. The linearised power law can then be rearranged into the expression shown in Eq. (14), which can be used with linear regression to obtain values for the A and n parameters, given a set of $\dot{\varepsilon}_m$ and σ values from the same temperature.

$$\ln(\dot{\varepsilon}_m) = n \ln(\sigma) + \ln(A) \tag{14}$$

Linear regression was conducted with the linearised power law using the creep data at 800° C for all stress conditions (60MPa, 65MPa, 70MPa, and 80MPa). The results are shown in Fig. B1, where A is represented by the intercept of the vertical axis, and n is represented as the gradient of the line. Thus, one can infer that the optimised A and n values are $e^{-35.693}$ (3.153×10^{-16}) and 7.2884, respectively.
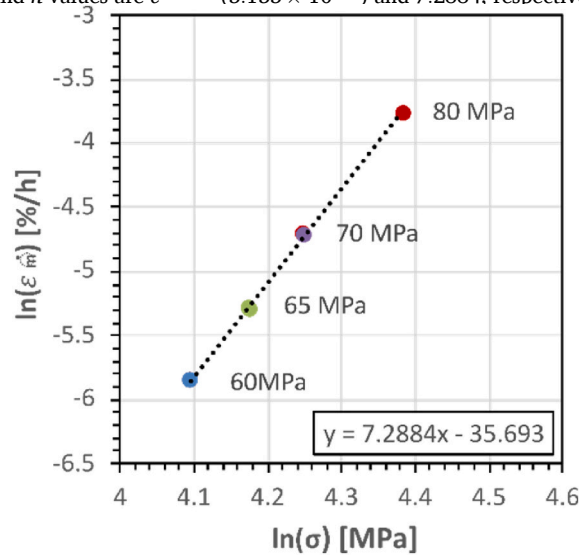

Fig. B1. Plot of the linearised Norton's power law using creep experimental data at 800 ° C, and stress conditions of 60MPa, 65MPa, 70MPa, and 80MPa.

Note that one needs at least three experimental datapoints (from three creep tests conducted at different stress conditions) to reliably apply the linearisation Norton's power law to obtain the values for the A and n parameters.

References

[1] R.E. Mizia, Next Generation Nuclear Plant Intermediate Heat Exchanger Acquisition Strategy, Office of Scientific and Technical Information (OSTI), 2008.

[2] W. Ren, R. Swindeman, A review on current status of alloys 617 and 230 for gen IV nuclear reactor internals and heat exchangers 1, J. Pressure Vessel Technol. 131 (4) (2009).

[3] J.K. Wright, Next Generation Nuclear Plant Intermediate Heat Exchanger Materials Research and Development Plan (PLN-2804), Office of Scientific and Technical Information (OSTI), 2008.

[4] W. Ren, R. Swindeman, A review paper on aging effects in alloy 617 for gen IV nuclear reactor Applications 1, J. Pressure Vessel Technol. 131 (2) (2008).

[5] F.H. Norton, The Creep of Steel at High Temperatures, McGraw-Hill book Company, 1929.

[6] F.R. Larson, J. Miller, A time-temperature relationship for rupture and creep stresses, Trans. ASME 74 (1952) 765–771.

[7] S.S. Manson, A.M. Haferd, U.S.N.A.C.f. Aeronautics, A Linear Time-Temperature Relation for Extrapolation of Creep and Stress-Rupture Data, National Advisory Committee for Aeronautics, 1953.

[8] R. Ainsworth, R5: an Assessment Procedure for the High Temperature Response of Structures, vol. 3, British energy generation Ltd, 2003.

[9] M.W. Spindler, The prediction of creep damage in type 347 weld metal. Part I: the determination of material properties from creep and tensile tests, Int. J. Pres. Ves. Pip. 82 (3) (2005) 175–184.

[10] Y. Takahashi, B. Dogan, D. Gandy, Systematic evaluation of creep-fatigue life prediction methods for various alloys, J. Pressure Vessel Technol. 135 (6) (2013).

[11] K. Kan, O. Muránsky, P.J. Bendeich, R.N. Wright, J.J. Kruzic, W. Payten, Assessment of creep damage models in the prediction of high-temperature creep behaviour of Alloy 617, Int. J. Pres. Ves. Pip. 177 (2019), 103974.

[12] L.M. Kachanov, The Theory of Creep (Teoriya Polzuchesti), National Lending Library for Science & Technology, 1967.

[13] I.N. Rabotnov, I.U.N. Rabotnov, I.U.r.N. Rabotnov, J.N. Rabotnov, Y.N. Rabotnov, F.A. Leckie, Creep Problems in Structural Members, North-Holland Publishing Company, 1969.

[14] W. Ren, Considerations of Alloy 617 Application in the Gen IV Nuclear Reactor Systems: Part I—Mechanical Property Challenges, ASME 2009 Pressure Vessels and Piping Conference, 2009, pp. 781–794.

[15] J.M. Garcia, L.P. Brandao, U.O. Costa, J.V. Salgado, L.F. Nunes, A.D.S. Paula, S. N. Monteiro, Experimental creep behavior and life prediction through observation and numerical analysis for AISI 310, J. Mater. Res. Technol. 9 (1) (2020) 222–229.

[16] C.M. Stewart, A.P. Gordon, Strain and damage-based analytical methods to determine the kachanov–rabotnov tertiary creep-damage constants, Int. J. Damage Mech. 21 (8) (2012) 1186–1201.

[17] C. Stewart, A. Gordon, Analytical Method to Determine the Tertiary Creep Damage Constants of the Kachanov-Rabotnov Constitutive Model, 2010.

[18] A. Ghatak, P. Robi, Prediction of creep curve of HP40Nb steel using artificial neural network, Neural Comput. Appl. 30 (2017) 2953–2964.

[19] J. Karthikeyan, A. Upadhyay, N.M. Bhandari, Artificial neural network for predicting creep and shrinkage of high performance concrete, J. Adv. Concr. Technol. 6 (1) (2008) 135–142.

[20] J. Zhong, C. Yang, W. Ma, Z. Zhang, Long-term creep behavior prediction of polymethacrylimide foams using artificial neural networks, Polym. Test. 93 (2021), 106893.

[21] S. Katoch, S.S. Chauhan, V. Kumar, A review on genetic algorithm: past, present, and future, Multimed. Tool. Appl. 80 (5) (2021) 8091–8126.

[22] T. Bartz-Beielstein, J. Branke, J. Mehnen, O. Mersmann, Evolutionary algorithms, WIREs Data Min. Knowl. Discov. 4 (3) (2014) 178–195.

[23] P.A. Vikhar, Evolutionary Algorithms: A Critical Review and its Future Prospects, IEEE.

[24] A. Chakraborty, A.K. Kar, Swarm Intelligence: A Review of Algorithms, Springer International Publishing, 2017, pp. 475–494.

[25] K. Sedighiani, M. Diehl, K. Traka, F. Roters, J. Sietsma, D. Raabe, An efficient and robust approach to determine material parameters of crystal plasticity constitutive laws from macro-scale stress–strain curves, Int. J. Plast. 134 (2020), 102779.

[26] J.K. Wright, L.J. Carroll, R.N. Wright, Creep and creep-fatigue of alloy 617 weldments medium, in: Idaho National Lab. (INL), Idaho Falls, ID (United States), Size, 2014, p. 50.

[27] J. Wright, Draft ASME Boiler and Pressure Vessel Code Case for Use of Alloy 617 for Class A Elevated Temperature Service Construction, INL/EXT-15-36305, Idaho National Laboratory, 2015.

[28] T.M. Lillo, R.N. Wright, Microstructural Characterization of Alloy 617 Crept into the Tertiary Regime, ASME 2015 Pressure Vessels and Piping Conference, American Society of Mechanical Engineers, 2015.

[29] J.K. Benz, L.J. Carroll, J.K. Wright, R.N. Wright, T.M. Lillo, Threshold stress creep behavior of alloy 617 at intermediate temperatures, Metall. Mater. Trans. 45 (7) (2014) 3010–3022.

[30] C. Jang, D. Lee, D. Kim, Oxidation behaviour of an Alloy 617 in very high-temperature air and helium environments, Int. J. Pres. Ves. Pip. 85 (2008) 368–377.

[31] D. Kim, C. Jang, W.S. Ryu, Oxidation characteristics and oxide layer evolution of alloy 617 and haynes 230 at 900 °C and 1100 °C, Oxid. Metals 71 (5–6) (2009) 271–293.

[32] J. Benz, R.N. Wright, Fatigue and Creep Crack Propagation Behaviour of Alloy 617 in the Annealed and Aged Conditions, 2013.

[33] P.J. Ennis, W.J. Quadakkers, H. Schuster, Effect of selective oxidation of chromium on creep strength of Alloy 617, Mater. Sci. Technol. 8 (1) (1992) 78–82.

[34] J. Blank, K. Deb, Pymoo: multi-objective optimization in Python, IEEE Access 8 (2020) 89497–89509.

[35] R.N. Greenwell, J.E. Angus, M. Finck, Optimal mutation probability for genetic algorithms, Math. Comput. Model. 21 (8) (1995) 1–11.

[36] A. Hassanat, K. Almohammadi, E.A. Alkafaween, E. Abunawas, A. Hammouri, V.B. S. Prasath, Choosing mutation and crossover ratios for genetic algorithms—a review with a new dynamic approach, Information 10 (12) (2019) 390.

[37] Y. Lin, W. Yang, Application of multi-objective genetic algorithm based simulation for cost-effective building energy efficiency design and thermal comfort improvement, Front. Energy Res. 6 (25) (2018).

[38] Z. Wang, O. Muránsky, H. Zhu, T. Wei, A. Sokolova, K. Short, R.N. Wright, On the kinetics of gamma prime (γ') precipitation and its strengthening mechanism in Alloy 617 during a long-term thermal aging, Materialia 11 (2020), 100682.